HYDROGELS

Hydro-locking in hydrogel for extreme temperature tolerance

Xiaochen Zhang[1]†, Dong Li[1]†, Xuxu Yang[2,3,4,5]†*, Lei Wang[1], Guo Li[1], Tuck-Whye Wong[2], Tiefeng Li[2,3,5]*, Wei Yang[2], Zisheng Luo[1,4]*

Hydrogels consist of cross-linked polymers that are highly swollen with water. Water evaporation or freezing during temperature changes may lead to stiff and brittle hydrogels. We introduce a strategy called "hydro-locking," which involves immobilizing the water molecules within the polymer network of the hydrogel. This is accomplished by establishing robust connections between water molecules and the polymer by using sulfuric acid. A sacrificial network is introduced to shield the prime polymer network from collapsing. Under the hydro-locking mode, an alginate-polyacrylamide double-network hydrogel remains soft and stretchable within a temperature range that spans from −115° to 143°C. The strategy works with a range of hydrogels and solutions and may enable the preservation and observation of materials or even living organisms at extreme temperatures.

Hydrogels, composed of water-filled cross-linked polymer networks, have been studied and used in tissue engineering (*1*, *2*), flexible electronics (*3*, *4*), and soft robotics (*5*, *6*). Enhancements in polymer networks have rendered hydrogels highly stretchable and tough (*7*–*9*). However, unlike elastomers with intrinsic entropic elasticity, hydrogels rely on the presence of mobile water molecules for their flexibility (*10*). Consequently, such dependency causes hydrogels to become stiff and brittle when subjected to water loss through evaporation or freezing during temperature change.

Locking water molecules within the polymer network of a hydrogel and maintaining its mobility are crucial for preserving the mechanical properties of the hydrogel across a broad temperature range (*10*). Current approaches involve substituting water with other liquids, increasing the phase transition temperature of the hydrogels. These solvents include ionic liquids (*11*) and aqueous solutions of inorganic salts (*12*, *13*), nonvolatile organic compounds such as trehalose (*14*), zwitterionic osmolytes (*15*), and combinations thereof (*16*, *17*). Ionic liquid gels exhibit a wide temperature range; however, they tend to absorb moisture from the air, leading to performance degradation over time (*18*, *19*). Aqueous solutions can incorporate additional components to raise the energy barrier for water transformation from a disordered to an ordered ice structure (*20*), reducing the freezing temperature of the solvent, typically between −20° and −80°C. The freezing temperature of the substituted solvent thus determines the lower temperature boundary of the hydrogel. Because water boils at 100°C at ambient pressure, the upper temperature threshold of hydrogels in these aqueous systems typically remains below 80°C (*16*, *21*). In hydrogels of substituted solvents, the water molecules are still mobile, leaving risks for their transition into ice or departure from the hydrogel, rendering the polymer network fragile.

[1]College of Biosystems Engineering and Food Science, Key Laboratory of Ago-Products Postharvest Handling of Ministry of Agriculture and Rural Affairs, Zhejiang University, Hangzhou, China. [2]Center for X-Mechanics, Department of Engineering Mechanics, Zhejiang University, Hangzhou, China. [3]State Key Laboratory of Fluid Power and Mechatronic Systems, Hangzhou, China. [4]Innovation Center for Postharvest Agro-Products Technology, Zhejiang University, Hangzhou, China. 5Institute of Fundamental and Transdisciplinary Research, Zhejiang University, Hangzhou, China.
*Corresponding author. Email: xxyang@zju.edu.cn (X.Y.); litiefeng@zju.edu.cn (T.L.); luozisheng@zju.edu.cn (Z.L.)
†These authors contributed equally to this work.

Design and preparation for hydro-locking

In this study, we achieved the stabilization of hydrogels at temperatures that surpass the typical liquid-phase temperature range of aqueous solutions through complete "hydro-locking," in which a majority of the water molecules are securely immobilized within the polymer network of the hydrogel, preventing their departure or transformation into ice. Sulfuric acid (H_2SO_4) demonstrates robust binding capabilities to water (*22*), as well as to polymers through ionic interactions and hydrogen bonds (Fig. 1A) (*23*). A single H_2SO_4 molecule can form multiple hydrates, with the binding energy surpassing 60 kcal mol^{-1} for hexahydrate (*22*). At elevated concentrations, H_2SO_4 can dehydrate hydrogen and hydroxy groups within polymer networks (*24*). During this dehydration process, acidification and sulfating reactions occur, and H_2SO_4 binds to polymers by displacing protonable groups, such as hydroxy groups, on the polymer chains (*25*).

We used an alginate-polyacrylamide double-network hydrogel (DN-gel) as the model material and treated it with H_2SO_4 to demonstrate the hydro-locking strategy (Fig. 1A). The DN-gel was initially immersed in H_2SO_4 solutions of varying concentration to create sulfuric hydrogel (S-gel). During immersion, H_2SO_4 reacts with the polymer chains, particularly alginate, leading to hydrolysis of glycosidic linkages and sulfation of hydroxy groups. Meanwhile, the H_2SO_4 molecules are connected on the surface of the polymer chains, spatially extending the area where the polymer could lock water molecules and accomplishing it by forming H_2SO_4 hydrates. The reactions generate fragments and branched structures of glycosyl polymer chains (Fig. 2A). Subsequently, we carbonized the S-gel in a 60°C oven for more than 48 hours, resulting in a fully carbonized sulfuric hydrogel (CS-gel). In the CS-gel, alginate chains degraded further, forming carbon dots that attach to and cover the main polyacrylamide chains, preventing it from overreaction with H_2SO_4 and collapse (Fig. 3).

Characterization and validation of hydro-locking

Hydro-locking induces a delay in the phase transition of all components within the hydrogel. Differential scanning calorimetry (DSC) results revealed a singular glass transition event for both S-gel and CS-gel, occurring at glass transition temperatures (T_g) of −123° and −115°C, respectively (Fig. 1B). This phase transition temperature is 42°C lower than the lowest freezing temperature (T_f) recorded for the H_2SO_4-H_2O binary system (*26*). The H_2SO_4 solution exhibited a tendency to avoid nucleation at low temperatures (*27*), aligning with the characteristic of hydrogel to inhibit nucleation (*28*), which contributes to the low phase-transition temperature. Hydro-locking also eliminates the evaporation of water from the hydrogel. DSC results showed an exothermic peak, with an onset temperature at 143°C, instead of an endothermic peak. A wide endothermic peak followed at >300°C that corresponded to the evaporation of the H_2SO_4-H_2O binary solution (Fig. 1B). These results demonstrated that the hydrogel did not exhibit a phase transition across a temperature range from −115° to 143°C.

We validated the success and impact of hydro-locking with a comparative analysis of a series of S-gels on their phase-transition behaviors (Fig. 1C). At lower H_2SO_4 concentrations, as seen in the S10 gel (the number indicates the H_2SO_4 concentration), we observed two peaks, at −3°C (T_{f1}) and −76°C (T_{f2}). As the H_2SO_4 concentration increased, as seen in the S20 and S30 gels, two endothermic peaks appeared above −50°C (T_{f1}) and around −73°C (T_{f2}), along with an exothermic peak connected to T_{f2} representing the cold crystallization process (T_{cc}) and a T_g at around −120°C. T_{f1} is associated with the ice crystallization, which diminishes with increasing H_2SO_4 concentration (Fig. 1D). The area of this peak, with higher H_2SO_4 concentration, decreases to 2.15% of S10 at S30 gel, indicating reduced overall water mobility (details and molar ratio analysis based

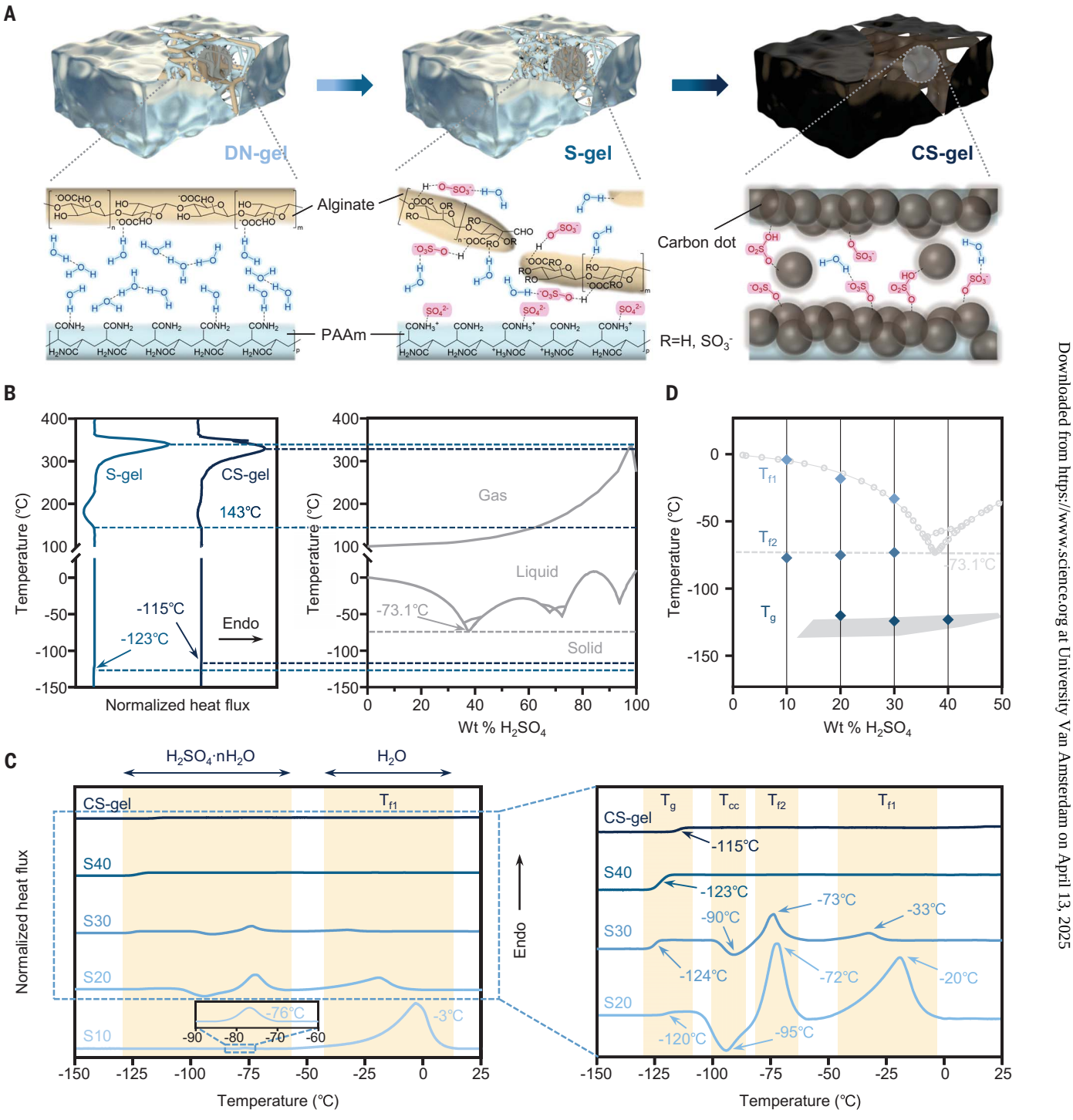

Fig. 1. Hydro-locking strategy and the phase transition temperature of S-gels. (**A**) A double-network hydrogel has a large proportion of free water among their polymer networks. H_2SO_4 molecules lock all water molecules on the polymer networks of hydrogels. (**B**) DSC measurements of S-gel and CS-gel demonstrate that no phase transition occurs between −115° and 143°C. The temperature range exceeds that of the liquid state of the binary H_2SO_4-H_2O system. (**C**) DSC measurements of various hydrogels from −150° to 25°C. The temperature regions of the glass transition (T_g), cold crystallization (T_{cc}), and freezing (T_{f1} and T_{f2}) are highlighted. The disappearance of these peaks signifies a reduction in free water molecules. (**D**) Comparison of thermodynamic events with phase diagram of the H_2SO_4-H_2O system from −175° to 25°C. Diamonds indicate the T_g and T_f emphasized in (C). The phase change progresses of the binary H_2SO_4-H_2O system are indicated in gray. Circles inidcate ice transition (*26*). The dashed line indicates the lowest freezing temperature of the binary H_2SO_4-H_2O system as a eutectic melting of ice and H_2SO_4 hydrates (*27*). The shaded area indicates the range of T_g for the binary H_2SO_4-H_2O system (*37*).

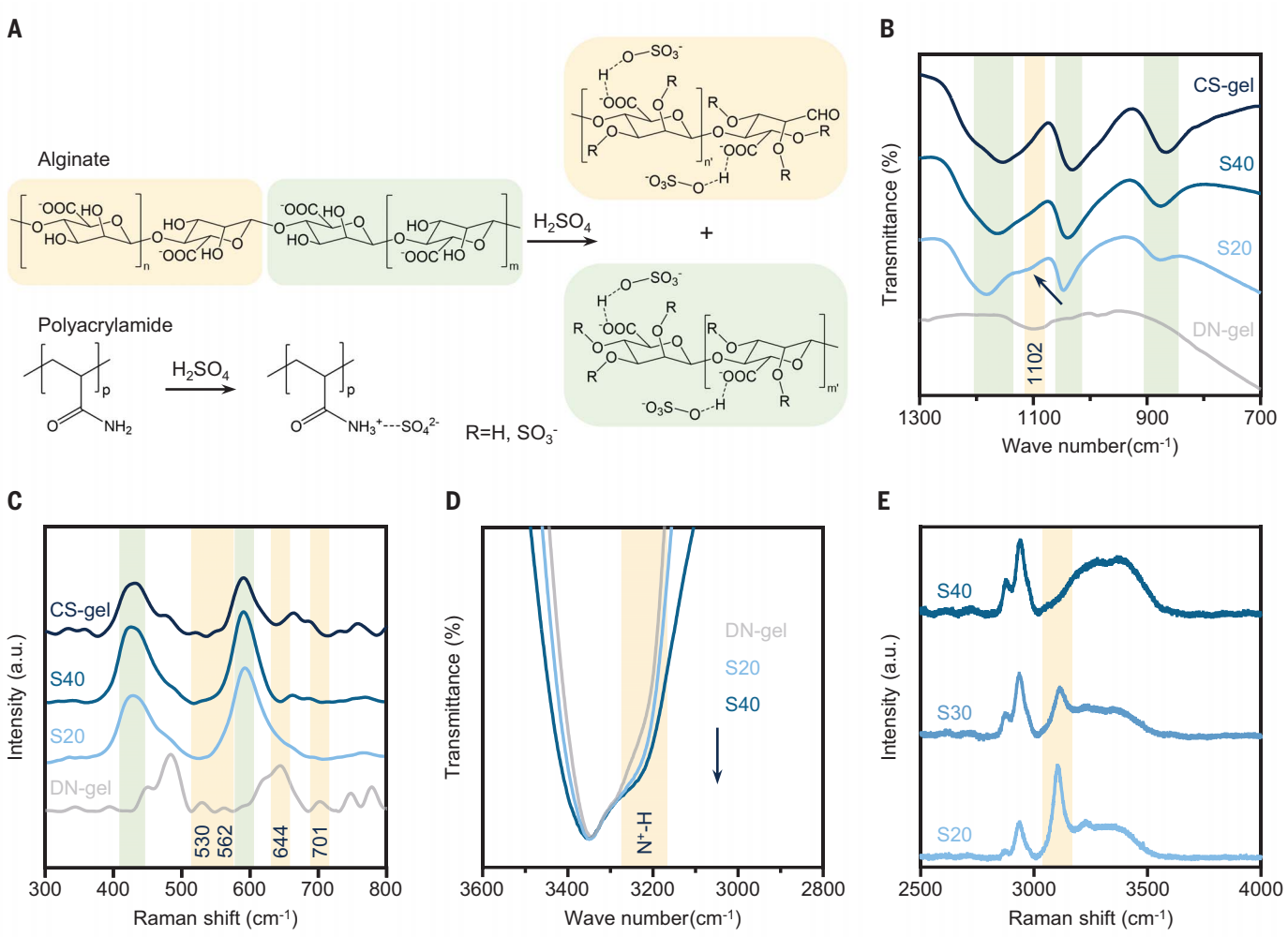

Fig. 2. Reactions and interactions in S-gels. (**A**) Chemical structures of alginate and polyacrylamide and structure alterations of them after treated with H_2SO_4. (**B**) FTIR spectra of DN-gel, S20, S40, and CS-gel in the range of 700 to 1300 cm^{-1}. The shoulder peak in S20 assigned to C–O stretching is indicated with an arrow, and the peaks related to H_2SO_4 are indicated in green. (**C**) Raman spectra of S20, S30, S40, and CS-gels from 300 to 800 cm^{-1}. The peaks related to HSO_4^- and/or SO_4^{2-} ions are indicated in green. (**D**) FTIR spectra of DN-gel, S20, and S40 in the range of 2800 to 3600 cm^{-1}. In (B) to (D), the changes in the peak intensity highlighted in yellow characterize [(A), top] the hydrolysis of alginate and [(A), bottom] the acidification of polyacrylamide. They exhibit a concentration-dependent manner, indicating stronger reactions and acidification upon increased acidity. (**E**) Raman spectra of S20, S30, and S40 gels at −130°C from 2500 to 4000 cm^{-1}. The highlighted area indicates the peak for $-NH_2$ symmetric stretching. The disappearance of this peak indicates that $-NH_2$ groups are being grafted by H_2SO_4 hydrates.

on the enthalpy changes acquired from the DSC diagrams and the heat of fusion for H_2O and H_2SO_4 hydrates are provided in the supplementary text, with results in table S1). T_{f2} matches the phase-transition temperature of H_2SO_4 hydrates (*27*, *29*). The area of this peak initially increases around 24-fold with the rise in H_2SO_4 concentration from S10 to S20 and then decreases to about 27% of its value at S20 as the concentration further increases from S20 to S30. The emergence of T_g signifies the creation of a new phase, which we posit as being the H_2SO_4 hydrates grafted onto the polymer network. At sufficiently high H_2SO_4 concentrations, as in the S40 gel, the peaks of T_{f1}, T_{f2}, and T_{cc} disappeared, and only the T_g remains. In this case, an adequate amount of H_2SO_4 molecules serve as anchors, connecting both the water molecules and the polymer chains. Therefore, a vast majority of water molecules are locked by H_2SO_4 as H_2SO_4 hydrates and grafted onto the polymer network of the hydrogel.

Fourier transform infrared (FTIR) and Raman spectroscopy helped to identify the reactions and acidification during the forge of hydro-locking (Fig. 2, B to D). In the FTIR spectra, the intensity of the peak at around 1102 cm^{-1} for C–O stretching in CH–OH reduces evidently in S-gels, indicating the hydrolysis of alginate. The process can also be characterized by the reduction of the peaks in Raman spectra at 644 and 701 cm^{-1} for symmetrical stretching of ring deformation and glycosidic linkage, along with the peaks at 530 and 562 cm^{-1} for the deformation vibration of C–C–C and C–O–C. The hydrolysis of alginate not only binds sulfate groups onto the polymer networks and extends the area of locking water molecules spatially but also facilitates the sacrifice of alginate during the protective carbon layer formation at the later carbonization process. The H_2SO_4 molecules are also connected to the polymer chains through ionic interactions based on acidification. Such a process produces acidified gzroups such as amide cation, resulting in a shoulder peak in the FTIR spectra near 3200 cm^{-1} assigned to the stretching vibration of N^+–H.

The hydro-locking was further validated by detecting the binding status of water on the

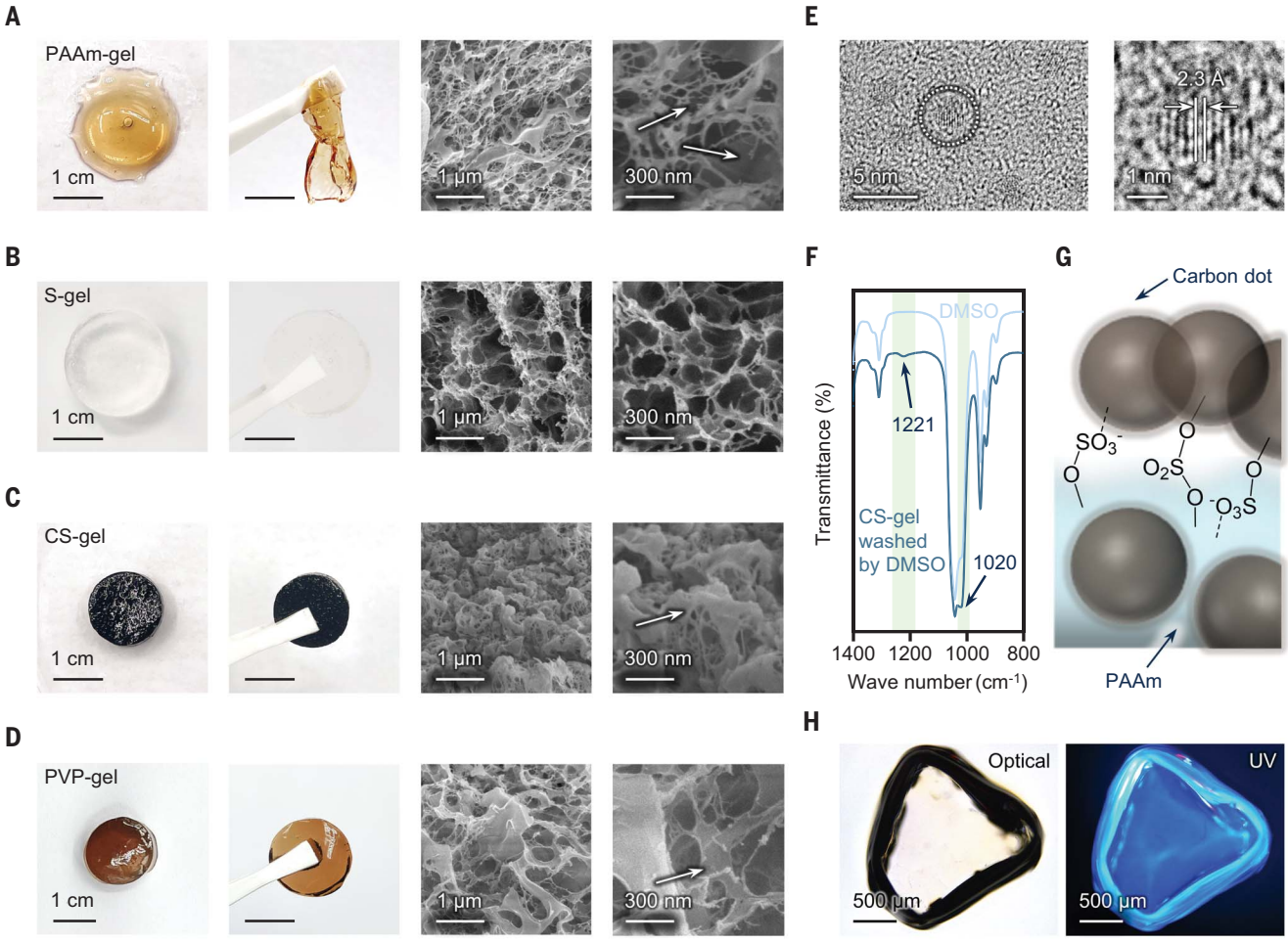

Fig. 3. Structure properties of S-gels and in situ carbon dots. (**A** to **D**) Optical and scanning electron microscope (SEM) images illustrating the microscope morphology of polymers in (A) PAAm-gel after treating with H_2SO_4 and heating in an oven at 60°C, (B) S-gel, (C) CS-gel, and (D) PVP hydrogel after treating with H_2SO_4 and heating in an oven at 60°C (PVP-gel). The arrows indicate the discontinuous filaments in PAAm-gel and protective carbon layer in CS-gel and PVP-gel. (**E**) Transmission electron microscopy images of carbon dots extracted from the CS-gel. (**F**) FTIR spectra of CS-gel washed by DMSO and DMSO from 800 to 1400 cm^{-1}. The peaks at 1020 cm^{-1} and 1221 cm^{-1} indicate the organo sulfate groups, which (**G**) connect carbon dots to the PAAm chains. (**H**) Optical and UV images of CS-gel washed with DMSO. The images were obtained with an inverted fluorescence microscope (Leica DMi8, Leica Biosystems, Germany) equipped with an excitation light source of 340 to 380 nm.

polymer chains at various temperatures. In the Raman spectra, a peak between 3100 and 3200 cm^{-1} represents $-NH_2$ symmetric stretching in the acrylamide monomer. This group is typically obscured by water or other solvent molecules through hydrogen bonding, rendering it undetectable (*30*). Only upon the full detachment of solvent molecules from polymer networks by freezing does $-NH_2$ become exposed, allowing the peak to manifest (fig. S1A). The presence of this peak serves as an indicator of the binding state of polymer with the solvent molecule, which is typically water and, in this case, also H_2SO_4 hydrates. Raman spectroscopy of the S-gels was conducted at various temperatures (Fig. 2E and fig. S1). In the presence of ample free water, as in S20, $-NH_2$ covered by free water was exposed at −50°C when the water freezes. By increasing the H_2SO_4 concentration, water molecules were captured by H_2SO_4, forming H_2SO_4 hydrates. Hence, the peak of $-NH_2$ symmetric stretching remained indistinct at −50°C but appeared at −100°C and lower temperatures. In S40, the peak of NH_2 symmetric stretching did not emerge at any tested temperature. This is attributed to the strong connections forged between $-NH_2$ groups and H_2SO_4 hydrates. The covering of H_2SO_4 hydrate persisted even at a temperature of −130°C, which is below the T_g of S40, when the entire system vitrifies.

At elevated temperatures, the CS-gel undergoes a phase transition at around 140°C, which diverges from conventional hydrogels that typically desiccate at the water boiling point of 100°C.

Thermogravimetric analysis (TGA) and DSC analysis were performed to investigate the difference (figs. S2 and S3). Heating from 30°C, the H_2SO_4 exhibits varying water absorption capacities, and the H_2SO_4 solution is gradually concentrated as the H_2SO_4 hydrates lose bound water. Each temperature corresponds to a different water content in the hydrogel once the hydrogel achieves equilibrium, thus locking in different amounts of water. The boiling point of the H_2SO_4 solution increases with the solution concentrating and reaches higher than that of water, so the concentrating process continues above 100°C. At around 140°C, we observed an exothermic peak in the DSC curve of

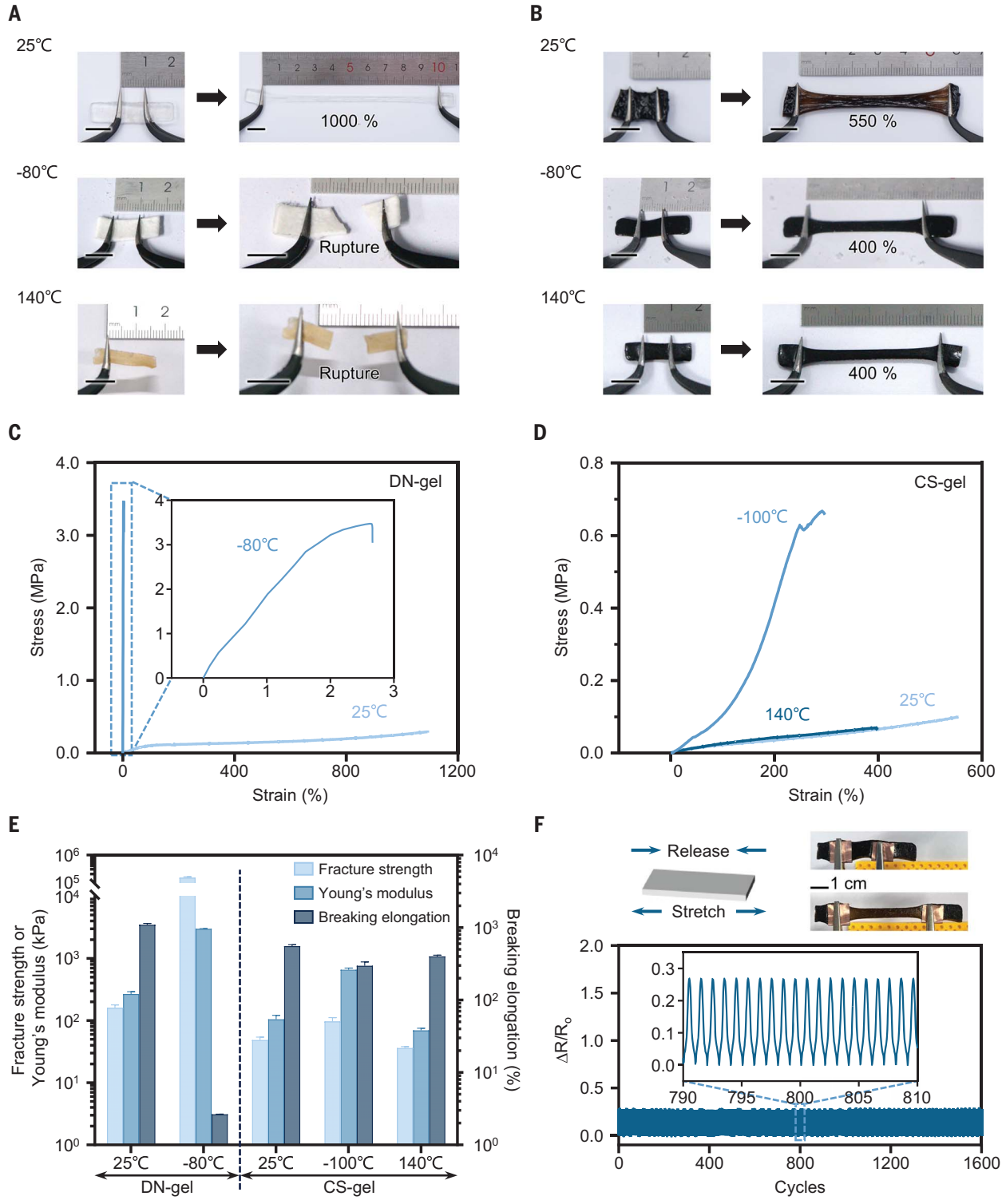

Fig. 4. Mechanical properties of CS-gel at extreme temperatures. (**A** and **B**) Optical images of (A) DN-gel and (B) CS-gel when stretched at 25°, −80°, and 140°C. (**C** and **D**) Tensile stress-strain curves of (C) DN-gel at 25° and −80°, and (D) CS-gel at 25°, −100°, and 140°C. (**E**) A comparison of fracture energy, Young's modulus, and breaking elongation of DN-gel at 25° and −80°, and CS-gel at 25°, −100°, and 140°C (n = 3 independent measurements). (**F**) Relative resistance ratio of the CS-gel when subjected to repeated stretch.

CS-gel, representing a degradation process rather than evaporation. We synthesized a series of CS-gels with varying contents of acrylamide and alginate, treated them with different concentrations of H_2SO_4 solutions, and carbonized them at temperatures ranging from 60° to 140°C. The reactions between H_2SO_4 and polymer components were consistent, resulting in almost identical onset temperatures of

the degradation process at around 140°C and peak temperatures at around 180°C. The reaction degrades the polymer components and generates products such as CO_2, which cause an additional decrease in mass.

Further investigations into the performance of CS-gels at temperatures exceeding 140°C reveals that at around 200°C, at which the exothermic peak has been passed, the reaction gradually slows down because the polymer network has collapsed. The decreasing rate of mass loss in the TGA results also slows down at around 200°C. The disrupted polymer networks fail to graft the H_2SO_4 hydrate, causing it to leak, forming cavities inside the hydrogels, and the hydrogel dries into a sponge-like structure (fig. S4). The H_2SO_4 solution that leaks from the hydrogel gradually evaporates and becomes more concentrated as the temperature rises. The concentrating continues beyond 300°C, the highest boiling point of the H_2SO_4-water binary solution (*31*), generating a strong endothermic peak at around 300°C (Fig. 1B and fig. S3).

Protective carbon dot layer in CS-gel

We used a DN-gel as the model hydrogel to prevent network collapse during the reaction with H_2SO_4 (Fig. 3 and fig. S5). In a single-network hydrogel of polyacrylamide, treating and reacting with H_2SO_4 at 60°C leads to chain cleavage, network fragmentation into discontinuous filaments, and degradation into a viscous liquid (Fig. 3A). However, in a DN-gel, the alginate network sacrificially reacts with H_2SO_4, creating a carbon shield around the acrylamide network (Fig. 3C). This sacrificial process occurs during the heat treatment, changing the hydrogel from transparent to black as carbon attaches to the remaining networks, preventing further degradation and leaving a higher proportion of the amino group from the polyacrylamide (fig. S6). The generation of carbon is proportional to the content of alginate (fig. S7) and affects the mechanical properties of the DN hydrogel. After treatment, a DN gel with 1.5 wt % alginate and 21 wt % polyacrylamide exhibits a modulus of 48.6 kPa and a stretchability of 5.34-fold (fig. S8 and table S2).

We used dimethyl sulphoxide (DMSO) to remove the free H_2SO_4 in the CS-gel and compared it with DMSO in the FTIR spectra (Fig. 3F and fig. S9). Although the peaks at 1160 and 876 cm^{-1} representing free H_2SO_4 are absent, in the FTIR spectra of the DMSO-washed CS-gel we observed peaks at 1020 cm^{-1} contributing to the S–O–C group of sulfate ester and at 1221 cm^{-1} contributing to the $-SO_3^-$ group of organo metal sulfate. The FTIR spectra revealed that the surface of the remaining acrylamide network is covered by smooth carbon based on the organo sulfate groups. We observed the generated carbon to be in the form of carbon dots (*32*), with diameters ranging from 1.98 to 4.06 nm in a weighted arithmetic mean measured with a Zetasizer (fig. S10). We observed the in-plane lattice spacing of the (100) facet of graphite, and the distinguishable lattice fringes (2.3 Å) of carbon dots was highlighted (Fig. 3E). These carbon dots protect the polymer networks (Fig. 3G) and exhibit fluorescence (Fig. 3H and fig. S11).

Generality for hydro-locking strategy

The hydro-locking strategy can be achieved with solutions other than H_2SO_4 and is applicable to various hydrogels. DMSO is a widely used biocompatible solvent in life science and can form strong hydrogen bonds with water and the hydrophilic groups on polymer networks (*33*). We treated the DN-gel with DMSO solutions (figs. S5E and S12A) and found that the hydrogel exhibited an extended functional temperature range with increasing DMSO concentration. We detected a broad functional temperature range expending to −125°C at a DN-gel treated with a 60 wt % DMSO solution. We also used the 60 wt % DMSO solution to treat the CS-gel. Such a treatment not only prevents the potential damage that may be caused by the H_2SO_4 on the surface of the CS-gel but also maintains the wide functional temperature range of the CS-gel (fig. S13).

We also demonstrated the strategy using a poly(*N*-vinylpyrrolidone) (PVP) hydrogel (Fig. 3D and figs. S5 and S12). A single network hydrogel typically collapses during the treatment of H_2SO_4 (Fig. 3A). However, PVP hydrolyzes in an acidic medium, leading to the breaking of an amide bond (*34*). The reactive side chain of PVP hydrolysis in the presence of H_2SO_4 (fig. S14) will further be carbonized during treatment below 60°C in an oven (Fig. 3D). The carbons cover the main chains of the polymer to prevent them from collapsing under continuous high temperature. Consequently, the PVP hydrogel has an extended functional temperature range from −112° to 135°C. (fig. S12B). The DMSO-treated PVP hydrogel showed similar results with a functional temperature range expanded to −122°C (fig. S12A).

Stretchability of CS-gel at extreme temperature

Hydro-locking in hydrogels maintains their softness and high stretchability under extremely low and high temperatures. We conducted tensile tests using a dynamic thermomechanical analyzer (DMA) (Fig. 4). We also tested a DN-gel for comparison, representing the mechanical properties of most tough hydrogels. At room temperature, the DN-gel exhibited excellent stretchability and toughness. However, after reaching equilibrium at low temperature (−80°C, held for 5 min in the DMA chamber), the DN-gel froze when the water within the polymer networks froze, becoming brittle. A similar phenomenon was observed at 140°C (the gels were preequilibrated in an oven for 24 hours at the required temperature, held for 5 min in the DMA chamber), where most water evaporated from the network, making the DN-gel crispy and distorted, rendering the sample barely stretchable (Fig. 4, A and C). We observed that the treatment with H_2SO_4 reduced the performance of the DN-gel, with the stretchability decreased to 50% (Fig. 4, D and E) and the toughness decreased to 30%. We attribute this performance degradation to the degradation of alginate and the decrease in the ionic cross-linker of the alginate network when the SO_4^{2-} combines with the cross-linker Ca^{2+}. The modulus and toughness of the hydrogel degrade when the cross-linker density and the energy dissipator decrease (*7*). However, their properties are better preserved in the CS-gel at extreme temperatures (Fig. 4D and fig. S15). A CS-gel undergoes an increase in modulus and a decrease in stretch limit but remains soft. The modulus of the CS-gel increased 1.1-fold from room temperature to −80°C and 1.8-fold from −80° to −100°C, owing to the exponential growth in the viscosity of H_2SO_4 hydrate with decreasing temperature (*35*). For better presentation, we preserved a CS-gel in a −80°C chamber for more than 24 hours, and it resisted stretching and twisting (Fig. 4B, fig. S16, and movie S1). At elevated temperatures as high as 140°C, the CS-gel retained its shape and stretchability (Fig. 4, B and D). The stress-strain curve of a CS-gel at 140°C is parallel to and slightly higher than that at 25°C (fig. S17). The modulus did not differ much from that at 25°C. When the influence of temperature was eliminated, the modulus increased significantly, indicating that the CS-gel softens at 140°C compared with 25°C (fig. S17 and supplementary text)

We also tested the stretchability of CS-gel at 140°C under an oil bath, which provides a stabler and more homogeneous thermal environment, and the test validated its thermal stability (fig. S18 and movie S2). The results demonstrate the softness of the CS-gel within the temperature range from −100° to 140°C. Our results were compared with recent works on hydrogel materials that tolerate wide temperature ranges, derived from nonvolatile organic solutions (NO), inorganic salts (IS), heterogeneous network organohydrogels (OH), ionic liquids (IL), or zwitterionic osmolytes (ZO) (fig. S19 and table S3).

Functionality and application

After washing the CS-gels, we captured a fluorescence image by exposing the hydrogel under ultraviolet (UV) light at 340 to 380 nm, showing a bright blue emission light with a peak emission wavelength at 461 nm (figs. S11 and S20). The color of the emission light also corresponds to the diameter of the carbon dots (fig. S10). The fwashing process lowers the concentration of

carbon dots to prevent quenching. Without the washing process, the gel was black, and the concentration of carbon dots was too high to generate a clear image (Fig. 3H and fig. S11A). Because the carbon dots originate from the reaction of alginate and H_2SO_4, the fluorescence intensity can be controlled by altering the alginate content (figs. S11, C to E, and S20C and movie S3).

The CS-gel can serve as a resistive strain-pressure sensor across an extended temperature range. During fabrication, conductive components, including sulfate ions and carbon dots, were introduced to the CS-gels. Consequently, the CS-gel exhibited a conductivity of about 1.27 S m^{-1} (fig. S21A). Maintaining stretchability over an extended temperature range, the CS-gel preserves its conductivity. Measurements from −80° to 140°C show that the CS-gel retains 22.17% of the conductivity at −20°C and 0.07% at −80°C. At elevated temperatures, conductivity increases, reaching 3.26 S m^{-1} at 140°C. The temperature-dependent behavior of conductivity correlates with the characteristics of a semiconductor, in which electron mobility increases with temperature (*36*). We applied mechanical loadings to the hydrogels within an electric circuit. Relative resistance alteration (ΔR), with ΔR representing the difference between the real-time resistance R and the initial resistance R_0, was measured. Stretching and pressing increased ΔR, which diminished if the load was released (Fig. 4F and fig. S21B). $\Delta R/R_0$ curves also displayed a clear step-like trend during step-by-step stretching-releasing cycles (fig. S21C). In cyclic loading at an extended temperature range, $\Delta R/R_0$ changed smoothly and evenly (movies S4 and S5).

Summary

We demonstrated a strategy of hydro-locking in hydrogel by connecting the majority of water molecules to the hydrogel network. The hydrogel, with complete hydro-locking, exhibits strong stability in extreme temperatures and maintains its softness and stretchability in the range of −115°C to 143°C. This hydro-locking strategy is proved applicable to various hydrogels with appropriate connecting agents.

REFERENCES AND NOTES

1. K. H. Vining, D. J. Mooney, *Nat. Rev. Mol. Cell Biol.* **18**, 728–742 (2017).
2. M. A. English *et al*., *Science* **365**, 780–785 (2019).
3. T. Zhou *et al*., *Nat. Mater.* **22**, 895–902 (2023).
4. Y. Zhang *et al*., *Chem. Rev.* **123**, 11722–11773 (2023).
5. G. Li *et al*., *Nature* **591**, 66–71 (2021).
6. T. Li *et al*., *Sci. Adv.* **3**, e1602045 (2017).
7. J.-Y. Sun *et al*., *Nature* **489**, 133–136 (2012).
8. J. Gong, Y. Katsuyama, T. Kurokawa, Y. Osada, *Adv. Mater.* **15**, 1155–1158 (2003).
9. M. Hua *et al*., *Nature* **590**, 594–599 (2021).
10. L. X. Hou *et al*., *Adv. Mater.* **35**, e2300244 (2023).
11. Y. Ren *et al*., *Sci. Adv.* **5**, eaax0648 (2019).
12. Y. Lu *et al*., *InfoMat* **5**, e12409 (2023).
13. X.-F. Zhang *et al*., *Angew. Chem. Int. Ed.* **58**, 7366–7370 (2019).
14. Z. Han *et al*., *Sci. Adv.* **8**, eabl5066 (2022).
15. X. Sui *et al*., *Adv. Funct. Mater.* **30**, 1907986 (2020).
16. X. Dong *et al*., *Mater. Today* **72**, 25–35 (2024).
17. Z. Wang *et al*., *Research* **2020**, 1426078 (2020).
18. D. Zhao *et al*., *J. Mater. Chem. C Mater. Opt. Electron. Devices* **10**, 2732–2741 (2022).
19. H. Dong, A. A. Askalany, C. Olkis, J. Zhao, G. Santori, *Energy* **189**, 116186 (2019).
20. Q. Zhang *et al*., *Nat. Commun.* **11**, 4463 (2020).
21. H. Gao *et al*., *Nat. Commun.* **8**, 15911 (2017).
22. B. Temelso *et al*., *J. Phys. Chem. A* **116**, 2209–2224 (2012).
23. S. Zhou, C.-S. Li, X.-H. Fan, Z. Shen, *Polymer* **143**, 316–323 (2018).
24. C. Wang *et al*., *Bioresour. Technol.* **355**, 127251 (2022).
25. K. Yao, Q. Meng, V. Bulone, Q. Zhou, *Adv. Mater.* **29**, 1701323 (2017).
26. C. M. Gable, H. F. Betz, S. H. Maron, *J. Am. Chem. Soc.* **72**, 1445–1448 (1950).
27. K. D. Beyer, A. R. Hansen, M. Poston, *J. Phys. Chem. A* **107**, 2025–2032 (2003).
28. S. Li *et al*., *Research* **6**, 0190 (2023).
29. X. P. Morelle *et al*., *Adv. Mater.* **30**, e1801541 (2018).
30. M. K. Gupta, R. Bansil, *J. Polym. Sci., Polym. Phys. Ed.* **19**, 353–360 (1981).
31. D. Schwartz, R. Gadiou, J.-F. Brilhac, G. Prado, G. Martinez, *Ind. Eng. Chem. Res.* **39**, 2183–2189 (2000).
32. H. Choi *et al*., *Nat. Photonics* **7**, 732–738 (2013).
33. D. Lv *et al*., *J. Phys. Chem. A* **126**, 6882–6889 (2022).
34. M. T. Taghizadeh, S. Nasirianfar, *J. Polym. Sci. Technol.* **5**, 13–24 (2020).
35. L. R. Williams, F. S. Long, *J. Phys. Chem.* **99**, 3748–3751 (1995).
36. V. Coropceanu *et al*., *Chem. Rev.* **107**, 926–952 (2007).
37. T. Koop, *Z. Phys. Chem.* **218**, 1231–1258 (2004).

ACKNOWLEDGMENTS

The authors thank Z. Han. for advice in demonstration and Zhejiang University for assistance with SEM measurements. **Funding:** This work was supported by the National Natural Science Foundation of China, T2125009 (T.L.); the National Key R&D Program of China, 2023YFD2201300 (Z.L.); the National Natural Science Foundation of China, 12102388 (X.Y.); the National Natural Science Foundation of China, 92048302 (T.L.); the National Natural Science Foundation of China, 12321002 (X.Y.); the National Natural Science Foundation of China, 1247020271 (X.Y.); the National Key R&D Program of China, 2017YFA0701100 (T.L.); the Fundamental Research Funds for the Central Universities, 226-2022-00141 (T.L.); the Key Research and Development Project of Zhejiang Province, 2022C01022 (T.L.); the "Pioneer" R&D Program of Zhejiang, 2023C03007 (T.L.); and the Laoshan Laboratory, LSKJ202205300 (T.L.). **Author contributions:** Conceptualization: X.Z., D.L., X.Y., T.-W.W. Methodology: X.Z., D.L., X.Y., L.W., T.-W.W. Validation: X.Z., D.L., X.Y. Formal analysis: X.Z., D.L., X.Y. Investigation: X.Z., L.W. Resources: X.Y., Z.L., T.L. Data curation: X.Z. Writing – original draft: X.Z., D.L., X.Y., L.W. Writing – review & editing: X.Z., D.L., X.Y., T.-W.W., T.L., W.Y., Z.L. Visualization: X.Z., D.L., G.L. Supervision: X.Y., T.L., W.Y., Z.L. Project administration: X.Y., T.L., Z.L. Funding acquisition: X.Y., T.L., Z.L. **Competing interests:** Z.L., X.Z., X.Y., and D.L. are inventors on China National Intellectual Property Administration provisional patent application (202410167970.4) submitted by Zhejiang University that covers a preparation method of the conductive hydrogel tolerating extreme temperature. All other authors declare no competing interests. **Data and materials availability:** All data are available in the main text or the supplementary materials.

SUPPLEMENTARY MATERIALS

science.org/doi/10.1126/science.adq2711
Materials and Methods
Supplementary Text
Figs. S1 to S26
Tables S1 to S3
References (*38*–*59*)
Movies S1 to S5

Submitted 8 May 2024; resubmitted 28 August 2024
Accepted 3 January 2025
10.1126/science.adq2711